Editors' Suggestion

Long-Axis Spinning of an Optically Levitated Particle: A Levitated Spinning Top

J. A. Zielińska,[1] F. van der Laan,[1,2] A. Norrman,[1,3] R. Reimann,[1,4] M. Frimmer,[1] and L. Novotny[1,*]

[1]Photonics Laboratory, ETH Zürich, CH-8093 Zürich, Switzerland
[2]Center for Nanophotonics, AMOLF, 1098 XG Amsterdam, The Netherlands
[3]Center for Photonics Sciences, University of Eastern Finland, P.O. Box 111, FI-80101 Joensuu, Finland
[4]Quantum Research Center, Technology Innovation Institute, Abu Dhabi, United Arab Emirates

(Received 16 January 2024; accepted 6 May 2024; published 20 June 2024)

An elongated object can be rotated around one of its short axes, like a propeller, or around its long axis, like a spinning top. Using optically levitated nanoparticles, short-axis rotation and libration have been systematically investigated in several recent studies. Notably, short-axis rotational degrees of freedom have been cooled to millikelvin temperatures and driven into gigahertz rotational speeds. However, controlled long-axis spinning has so far remained an unrealized goal. Here, we demonstrate controlled long-axis spinning of an optically levitated nanodumbbell with spinning rates exceeding 1 GHz. We show that the damping rate in high vacuum can be as low as a few millihertz. Our results open up applications in inertial torque sensing and studies of rotational quantum interference.

DOI: 10.1103/PhysRevLett.132.253601

Introduction.—Cylindrically symmetric nanorotors, when trapped within linearly polarized optical tweezers, align their most-polarizable (long) axis to the polarization direction of the tweezers. This results in libration of the rotor, i.e., torsional oscillations around an equilibrium angle driven by a linear restoring torque. In particular, two degenerate libration modes emerge, corresponding to oscillatory rotations around the two least-polarizable (short) axes. Significant advances have been made in controlling short-axis rotations, with nanorotors being driven to spin at gigahertz rates [1–4], libration oscillations cooled down to millikelvin temperatures [5–8], and several demonstrations of torque sensing [3,9–12]. However, in all these studies the rotation around the long axis remained unconstrained and was driven by thermal fluctuations [5,6,13]. Introducing controlled long-axis spinning would complement the existing research on short-axis rotations by enabling the simultaneous control of the rotational rate and the orientation of the rotation axis. This achievement would close a notable gap in the field and provide a valuable resource for inertial torque sensing.

A levitated gyroscope with competitive performance requires large angular momentum and low friction, which poses constraints on vacuum pressure and rotor size [14,15]. Inertial torque sensing of rotations has been successfully demonstrated using levitated birefringent vaterite particles [14,16,17], but the relatively high absorption rate of these particles prevents optical trapping in ultrahigh vacuum (UHV). On the other hand, silica nanoparticles can withstand UHV conditions [18] and they can be fused together to generate particles with shape anisotropy, such as cylindrically symmetric dumbbells. Furthermore, silica nanorotors can be precisely controlled down to their fundamental quantum and thermodynamic limits [4,6] and driven to rotate at gigahertz rates around their short axes [1–4]. Nonetheless, gyroscope applications rely on accurately monitoring the orientation of the spinning axis of the rotor. This is not feasible for short-axis rotations, since the spinning axis aligns with the tweezer propagation direction and is not reliably detected [19]. Therefore, controlled spinning around the long axis is a key requirement for the realization of an optically levitated gyroscope, because it simultaneously enables fast spinning and accurate measurement of the spinning axis orientation.

Long-axis spinning is also an important resource for studying quantum interference in the orientational dynamics of nanorotors [20]. The angular momentum of a free quantum rotor is quantized and, in principle, it can be

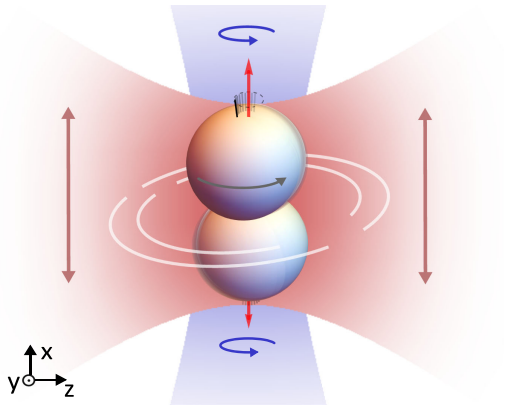

FIG. 1. A nanodumbbell (not to scale) is trapped by an x polarized laser beam (red) and spun around its long axis by a circularly polarized spinning beam (blue).

prepared in a single eigenstate [21]. Thanks to the cylindrical symmetry of the dumbbell, the spinning around the long axis is decoupled from other rotations and defines a "free rotational" degree of freedom with quantized angular momentum [21]. This is different from translational and librational modes, which are governed by harmonic dynamics or short-axis rotations that are coupled to each other. Thus, long-axis spinning is a prerequisite for the exploration of quantum rotational effects [20], such as rotational revivals [22].

System under study.—Our system, illustrated in Fig. 1, consists of an optically levitated nanodumbbell exposed to a light field in a three-dimensional (3D) polarization state [23,24]. The light field is composed of two parts: a strong tweezer field, linearly polarized along the x axis and propagating in the z direction, and a weak spinning beam, circularly polarized in the y-z plane and propagating along the x direction. The tweezer field exerts a conservative restoring torque on the dumbbell, which aligns its long axis in the x direction and creates two libration modes around this equilibrium. In contrast, the circularly polarized beam generates a constant (and therefore nonconservative) torque, which drives the dumbbell into a spinning motion around its long axis. This torque arises from the optical spin [25,26] carried by the beam together with absorption or imperfect cylindrical symmetry of the dumbbell [27–29].

The rotational dynamics of the nanodumbbell is thus governed by two libration angles φ and ϑ with respect to the x axis and the rotation angle ψ around its long axis (see Supplemental Material [30]). In the presence of friction and assuming small-angle libration, the dumbbell's spinning rate will accelerate until it reaches its steady-state value $\dot{\psi}_0 = \tau/(I_3\gamma_3)$ [1,2,4], where τ is the magnitude of the nonconservative torque, I_3 is the moment of inertia along the long axis, and γ_3 is the friction coefficient. The spinning motion reveals itself as a coupling $g = (I_3/2I_1)\dot{\psi}_0$ between the otherwise independent and harmonic libration modes, where I_1 is the moment of inertia along one short axis. The coupling leads to hybrid modes with eigenfrequencies

$$\Omega_{1/2} = \sqrt{\Omega_0^2 + g^2} \pm g, \tag{1}$$

where Ω_0 is the natural libration frequency [13,30]. The higher frequency Ω_1 corresponds to nutation of the long axis, whereas the lower frequency Ω_2 is associated with precession of the long axis around the x direction [11,13,38,39].

Most importantly, since the spinning rate is directly related to the torque and friction, with the torque scaling linearly with the spinning beam power [30], in our experimental implementation we can control the spinning rate via the optical power of the circularly polarized spinning beam and the chamber pressure. For high enough spinning rates, we can push our system far into the strong coupling regime, i.e., $g \gg \Omega_0$. In this regime we can approximate the eigenfrequencies as

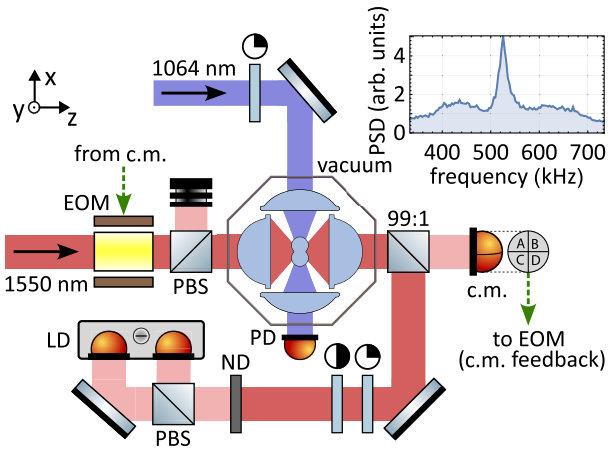

FIG. 2. Experimental apparatus for spinning a dumbbell. The x polarized optical tweezers (wavelength 1550 nm) trap a dumbbell inside a vacuum chamber, while a circularly polarized beam (wavelength 1064 nm) propagating along x spins the dumbbell. Forward scattered light from the tweezers is split and subsequently sent to a quadrant photodiode and a balanced detector for center of mass (c.m.) and libration detection (LD), respectively. The detected c.m. motion is used to drive an electro-optic modulator (EOM) for feedback cooling x and y c.m. motion. The power of the spinning beam is monitored on a photodiode (PD). Inset: power spectral density (PSD, plotted in arbitrary units) of the libration motion of a trapped dumbbell recorded at a pressure of 0.1 mbar and without the spinning beam.

$$\Omega_1 = 2g, \tag{2a}$$

$$\Omega_2 = \frac{\Omega_0^2}{2g}. \tag{2b}$$

As we increase the spinning rate of the dumbbell, the amplitude of nutation relative to precession decreases, and the motion becomes dominated by slow precession with frequency Ω_2 [40].

Experimental setup.—In our experiment, depicted schematically in Fig. 2, dumbbells composed of two spherical silica nanoparticles (nominal diameter 143 nm) are optically trapped inside a vacuum chamber. The particles are loaded into the trap using a nebulizer. The tweezer beam forming the trap (wavelength 1550 nm, power 700 mW) is focused with an NA = 0.8 lens. The light scattered by the particle is subsequently collected by an NA = 0.7 lens and analyzed to detect librations in the x-y plane and the c.m. motion along three main axes. For detecting the c.m. motion, we use a quadrant photodiode, while libration is recorded with the help of a polarizing beam splitter (PBS) and a balanced detector as in [6]. In order to stabilize the position of the dumbbell inside the trap, we cool the x and y c.m. motion by parametric feedback [41] at pressures below 10^{-4} mbar.

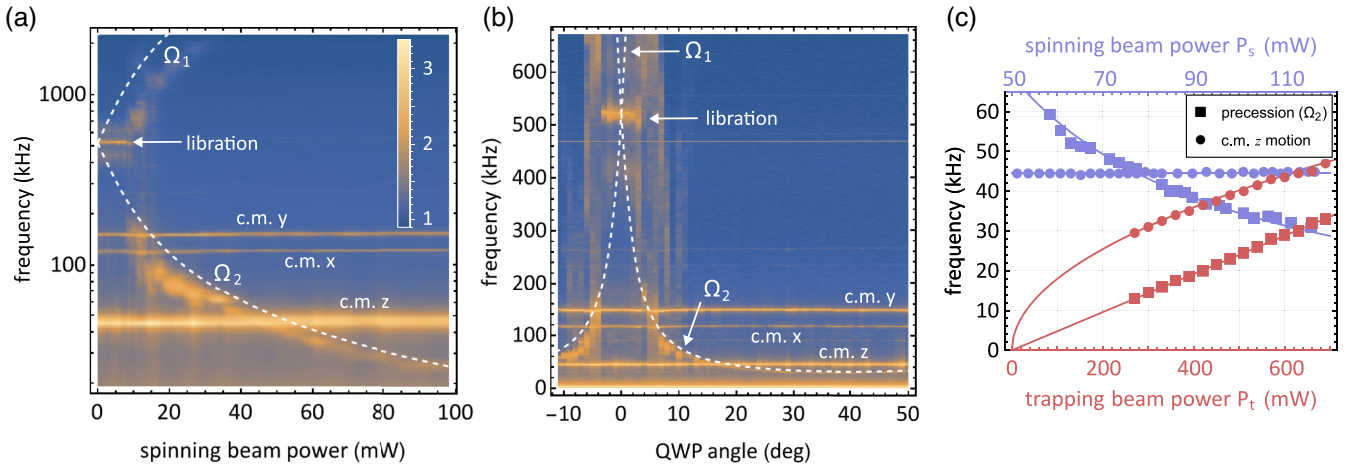

FIG. 3. PSD of the detector signal as a function of (a) spinning beam power and (b) spinning beam polarization. The color scale for (a) and (b) depicts log(PSD) in arbitrary units and the fits to Eq. (1) are shown as white dashed lines. Measurements (a)–(c) were performed at a pressure of 10^{-3} mbar. (a) As the spinning beam power is increased, the libration peak splits into a high frequency nutation mode (Ω_1) and a low frequency precession mode (Ω_2). (b) As the QWP angle is rotated from 0° to 45°, the spinning beam polarization changes from linear to circular and the libration mode evolves into a precession mode with frequency Ω_2. The spinning beam power is 100 mW. Note that the frequency scale is logarithmic in (a), whereas it is linear in (b). (c) Precession frequency Ω_2 and c.m. z-motion frequency as a function of trapping beam power (lower curves, spinning beam power 100 mW) and as a function of spinning beam power (upper curves, trapping beam power 700 mW). The spinning beam is circularly polarized. Solid lines show theoretically predicted behaviour of Ω_2 and c.m. z-motion frequencies.

We identify a trapped particle as a dumbbell when its c.m. x-to-y gas damping ratio is in the 1.1–1.15 range [2]. Another characteristic of dumbbells is their libration spectrum, which consists of a sharp libration peak at 525(3) kHz flanked by broad shoulders [5,6,13,42], as shown by the inset of Fig. 2.

The spinning beam (wavelength 1064 nm, tunable power up to 120 mW) is focused onto the dumbbell by an NA = 0.3 lens with 7.5 mm focal length. The beam is then collected by another NA = 0.3 lens and its power is monitored using a photodiode. The polarization state of the spinning beam is controlled by a quarter-wave plate (QWP). Because of its low power and weak focusing, the spinning beam does not significantly alter the libration potential [30].

Results.—Figure 3(a) shows the measured libration spectra for different optical powers of the circularly polarized spinning beam at 10^{-3} mbar. For powers below 10 mW the thermally driven spinning dominates, as evidenced by the constant libration frequency accompanied by the shoulderlike line shape on both sides (cf. inset in Fig. 2). As we increase the spinning beam power above the 10 mW threshold, the libration mode splits into two hybrid modes created by the spinning motion. The white dashed curves are theoretical fits according to Eq. (1) that qualitatively agree with the experimental observations. We observe a broad high frequency nutation peak (Ω_1) and a narrow low frequency precession mode (Ω_2). As expected, the frequency Ω_1 of the nutation mode increases and its amplitude decreases [40] with increasing spinning beam power. The observed behavior of Ω_2 frequency and Eq. (1) agree well for spinning beam powers above 40 mW, where the spinning rate of the dumbbell transitions into the fast spinning regime characterized by $g \gg \Omega_0$ [see also Fig. 3(c)]. Below 40 mW our model does not accurately predict the frequencies, including the 10 mW spinning beam power threshold for mode splitting (also reported in Ref. [42]). We believe these deviations are related to the factors not included in our model, such as coupling to the c.m. motion or imperfect shape of the dumbbell.

The torque τ experienced by the dumbbell can also be controlled by the polarization of the spinning beam. In Fig. 3(b) we show the measured libration spectra as a function of the QWP angle that changes the polarization of the spinning beam from linear to circular (see Fig. 2). When the QWP is set at 0°, the beam is linearly polarized in the z direction and has no detectable effect on the libration dynamics due to lack of optical spin. The coupling is dominated by thermally driven spinning, as if the spinning beam was absent. However, when the polarization becomes elliptical (QWP is rotated by approximately 5° in either direction) the dynamics transitions abruptly into consistent spinning, as evidenced by the emerging low frequency precession mode (Ω_2). For circular polarization, Ω_2 decreases to approximately 30 kHz. The minimum of the precession frequency occurs around 35° due to birefringence of the vacuum viewport (included in the fit).

Next, we investigate the dependence of the precession frequency Ω_2 on the trapping beam power P_t and the spinning beam power P_s in the fast spinning regime

($g \gg \Omega_0$). The natural libration frequency Ω_0 was shown to depend on the square root of P_t [13]. This implies, according to Eq. (2b), that the precession frequency Ω_2 depends linearly on P_t, as long as the coupling rate g is not affected by the trapping beam. The expected behavior is indeed confirmed by our measurements shown in Fig. 3(c). On the other hand, since the torque τ exerted on the dumbbell depends linearly on the spinning power P_s, we expect, according to Eq. (2b), that Ω_2 scales inversely with P_s. We compare the behavior of Ω_2 with that of the eigenfrequency of the c.m. z mode (which is expected to follow a square-root behavior on P_t and remain unaffected by changes in the spinning beam power P_s). The measured Ω_2 and c.m. z frequencies shown in Fig. 3(c) agree well with their respective predicted behaviors. We therefore conclude that Eq. (2b) correctly predicts the precession frequency in the fast spinning regime where $g \gg \Omega_0$. Note that the coupling strength surpasses the natural libration frequency even for moderate P_s, akin to deep ultrastrong coupling. According to Eq. (2b), the precession frequency of 30 kHz [see Figs. 3(a)–3(c)] corresponds to a coupling rate $g = 2\pi \times 4.6$ MHz. Assuming our dumbbells have a length-to-diameter ratio of 1.8 (as in Ref. [27]), we estimate $I_3/I_1 \approx 0.6$, which yields a spinning rate of $\dot{\psi}_0 \approx 2\pi \times 15$ MHz.

Ringdown measurements.—The steady-state spinning rate $\dot{\psi}_0 = \tau/(I_3\gamma_3)$ is inversely proportional to the damping rate γ_3, which, in turn, is proportional to the gas pressure. Thus, controlling the pressure allows us to tune $\dot{\psi}_0$ over several orders of magnitude. As described before, we can infer the dumbbell's spinning rate from the measured hybrid mode frequencies. However, in practice, we are only able to detect the precession mode Ω_2 for spinning rates up to $\dot{\psi}_0 \approx 30$ MHz. The reason for this is twofold: first, as $\Omega_2/(2\pi)$ decreases below 3 kHz it becomes obscured by electronic noise in our detection system [visible in Figs. 3(b) and 4(a)]; second, large spinning rates lead to large angular momenta that stabilize the system and reduce the precession amplitude, which results in poor signal-to-noise ratio in our measurements. We circumvent this problem by performing ringdown measurements, in which P_s is set to zero and the slowing down of the dumbbell's spinning rate is monitored [1]. For sufficiently high spinning rates, thermal fluctuations can be ignored and the ringdown turns into a deterministic trajectory described by $\dot{\psi}(t) = \dot{\psi}(0)e^{-\gamma_3 t}$. Consequently, according to Eq. (2b), the precession frequency exponentially increases in time as

$$\Omega_2(t) = \frac{\Omega_0^2}{2g(0)} e^{\gamma_3 t}. \tag{3}$$

Note that this description is valid for $g \gg \Omega_0$, and thus we only use Eq. (3) to determine $g(0)$, $\dot{\psi}(0)$, and γ_3 in this parameter regime.

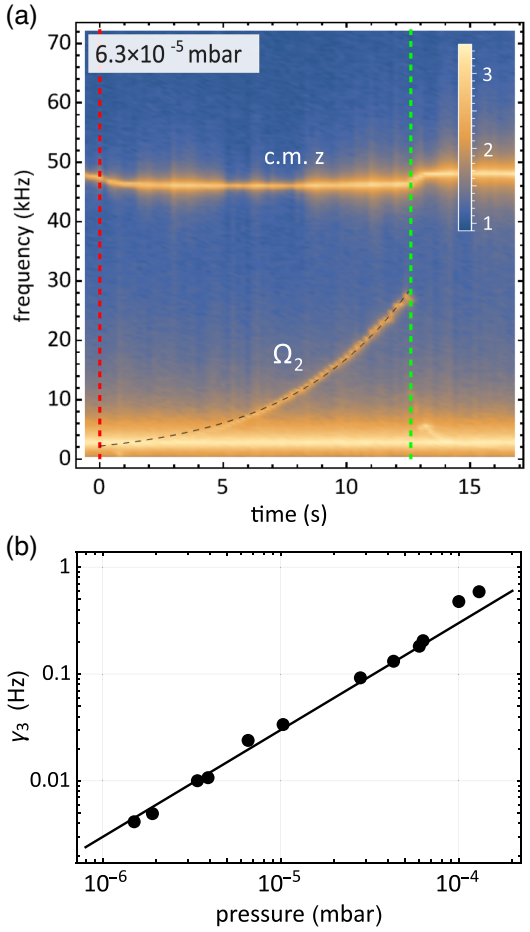

FIG. 4. Ringdown measurements for different pressures. (a) PSDs as a function of time t, after blocking the spinning beam (initial power 50 mW) at $t = 0$, marked by the dashed red line. The vacuum pressure is 6.3×10^{-5} mbar. The dumbbell's spinning rate decreases due to friction, which is evidenced by the increase of the precession mode frequency Ω_2. The time the spinning beam is switched back on is indicated by a dashed green line. Color shows log(PSD) in arbitrary units. (b) Damping rate γ_3 as a function of pressure extracted from ringdown measurements. Error bars are smaller than the size of the data points. The solid line is a linear fit.

Figure 4(a) shows a ringdown measurement performed at a pressure of 6.3×10^{-5} mbar. The spinning beam is switched back on at $t \approx 12.5$ s (green dashed line), before Ω_2 reaches the c.m. z frequency. The data show that Ω_2 increases exponentially after switching off the spinning beam. From a fit to Eq. (3), shown as a black dashed line, we extract the spinning rate $\dot{\psi}(0) = 2\pi \times 210(7)$ MHz and damping rate $\gamma_3 = 204(2)$ mHz, together with their standard errors.

We repeat similar ringdown measurements for even lower pressures, down to 1.5×10^{-6} mbar, where we reach the exceptionally high spinning rate of $\dot{\psi}(0) = 2\pi \times 1.20(6)$ GHz. The extracted damping rates γ_3, measured for pressures between 10^{-6} and 10^{-3} mbar,

are shown in Fig. 4(b) together with a linear fit [43]. Despite the gigahertz rotational rates reached, throughout our experiments we do not observe consistent particle deformations (see Supplemental Material [30]).

Conclusion.—We have experimentally achieved controlled spinning of an optically levitated nanodumbbell around its long axis and demonstrated gigahertz spinning rates and damping rates of a few millihertz. This demonstration is of interest for applications in inertial torque sensing. The parameters demonstrated in this Letter translate into a thermally limited gyroscope sensitivity (angular random walk) of $\Omega_{\mathrm{ARW}} = \sqrt{4k_B T\gamma}/(\sqrt{I_3}\dot{\psi}_0) \approx 4 \times 10^{-6}\ \mathrm{rad/s}/\sqrt{\mathrm{Hz}}$ [15], which is only 2 orders of magnitude larger than the self-noise of the best high-end gyroscopes [44]. Our experiment can be further optimized, e.g., by using larger dumbbells (considering the scaling of γ [43] and I_3 [40] with particle radius r, and assuming that $\dot{\psi}_0 \propto r^{-1}$, we find $\Omega_{\mathrm{ARW}} \propto r^{-2}$) or by lower vacuum pressures.

Our system is fully described by classical dynamics, but we note that recent advances have brought rotational levitodynamics close to the quantum regime [20,45]. The demonstration of long-axis spinning expands the understanding of the interaction of rotational degrees of freedom with light and provides an important step toward the observation of macroscopic quantum effects [20,22,46].

Furthermore, our system can also serve as a platform for studying deep-strong coupling between mechanical modes [47] since the coupling rate g between libration modes, introduced by long-axis spinning, is shown to be nearly 3 orders of magnitude larger than the natural libration frequency Ω_0, thereby outperforming the g/Ω_0 values reached with trapped atoms [48].

The authors thank C. Gonzalez-Ballestero, J. Harris, and members of the Photonics Laboratory for fruitful discussions. This research was supported by the European Union's Horizon 2020 research and innovation program under Grant Agreement No. [863132] (IQLev) and ETH Grant No. ETH-47 20-2. A. N. acknowledges support from the Research Council of Finland (Grants No. 354918 and No. 346518). F. v. d. L. was supported by the Netherlands Organisation for Scientific Research (NWO).

*www.photonics.ethz.ch

[1] R. Reimann, M. Doderer, E. Hebestreit, R. Diehl, M. Frimmer, D. Windey, F. Tebbenjohanns, and L. Novotny, GHz rotation of an optically trapped nanoparticle in vacuum, Phys. Rev. Lett. **121**, 033602 (2018).

[2] J. Ahn, Z. Xu, J. Bang, Y.-H. Deng, T. M. Hoang, Q. Han, R.-M. Ma, and T. Li, Optically levitated nanodumbbell torsion balance and GHz nanomechanical rotor, Phys. Rev. Lett. **121**, 033603 (2018).

[3] J. Ahn, Z. Xu, J. Bang, P. Ju, X. Gao, and T. Li, Ultrasensitive torque detection with an optically levitated nanorotor, Nat. Nanotechnol. **15**, 89 (2020).

[4] F. van der Laan, R. Reimann, A. Militaru, F. Tebbenjohanns, D. Windey, M. Frimmer, and L. Novotny, Optically levitated rotor at its thermal limit of frequency stability, Phys. Rev. A **102**, 013505 (2020).

[5] J. Bang, T. Seberson, P. Ju, J. Ahn, Z. Xu, X. Gao, F. Robicheaux, and T. Li, Five-dimensional cooling and nonlinear dynamics of an optically levitated nanodumbbell, Phys. Rev. Res. **2**, 043054 (2020).

[6] F. van der Laan, F. Tebbenjohanns, R. Reimann, J. Vijayan, L. Novotny, and M. Frimmer, Sub-kelvin feedback cooling and heating dynamics of an optically levitated librator, Phys. Rev. Lett. **127**, 123605 (2021).

[7] J. Schäfer, H. Rudolph, K. Hornberger, and B. A. Stickler, Cooling nanorotors by elliptic coherent scattering, Phys. Rev. Lett. **126**, 163603 (2021).

[8] A. Pontin, H. Fu, M. Toroš, T. S. Monteiro, and P. F. Barker, Simultaneous cavity cooling of all six degrees of freedom of a levitated nanoparticle, Nat. Phys. **19**, 1003 (2023).

[9] Z. Xu and T. Li, Detecting Casimir torque with an optically levitated nanorod, Phys. Rev. A **96**, 033843 (2017).

[10] S. Kuhn, B. A. Stickler, A. Kosloff, F. Patolsky, K. Hornberger, M. Arndt, and J. Millen, Optically driven ultra-stable nanomechanical rotor, Nat. Commun. **8**, 1670 (2017).

[11] M. Rashid, M. Toroš, A. Setter, and H. Ulbricht, Precession motion in levitated optomechanics, Phys. Rev. Lett. **121**, 253601 (2018).

[12] P. Ju, Y. Jin, K. Shen, Y. Duan, Z. Xu, X. Gao, X. Ni, and T. Li, Near-field GHz rotation and sensing with an optically levitated nanodumbbell, Nano Lett. **23**, 10157 (2023).

[13] T. Seberson and F. Robicheaux, Parametric feedback cooling of rigid body nanodumbbells in levitated optomechanics, Phys. Rev. A **99**, 013821 (2019).

[14] K. Zeng, X. Xu, Y. Wu, X. Wu, and D. Xiao, Optically levitated gyroscopes with a MHz rotating micro-rotor, arXiv:2308.09085.

[15] K. Poletkin, Mechanical thermal noise in levitation microgyroscopes, in *Levitation Micro-Systems: Applications to Sensors and Actuators* (Springer International Publishing, Cham, 2021), pp. 135–154.

[16] Y. Arita, M. Mazilu, and K. Dholakia, Laser-induced rotation and cooling of a trapped microgyroscope in vacuum, Nat. Commun. **4**, 2374 (2013).

[17] Y. Arita, S. H. Simpson, G. D. Bruce, E. M. Wright, P. Zemánek, and K. Dholakia, Cooling the optical-spin driven limit cycle oscillations of a levitated gyroscope, Commun. Phys. **6**, 238 (2023).

[18] L. Dania, D. S. Bykov, F. Goschin, M. Teller, and T. E. Northup, Ultra-high quality factor of a levitated nanomechanical oscillator, Phys. Rev. Lett. **132**, 133602 (2024).

[19] F. Tebbenjohanns, A. Militaru, A. Norrman, F. van der Laan, L. Novotny, and M. Frimmer, Optimal orientation detection of an anisotropic dipolar scatterer, Phys. Rev. A **105**, 053504 (2022).

[20] B. Stickler, K. Hornberger, and M. Kim, Quantum rotations of nanoparticles, Nat. Rev. Phys. **3**, 589 (2021).

[21] C. P. Koch, M. Lemeshko, and D. Sugny, Quantum control of molecular rotation, Rev. Mod. Phys. **91**, 035005 (2019).
[22] B. A. Stickler, B. Papendell, S. Kuhn, B. Schrinski, J. Millen, M. Arndt, and K. Hornberger, Probing macroscopic quantum superpositions with nanorotors, New J. Phys. **20**, 122001 (2018).
[23] A. Norrman, A. T. Friberg, J. J. Gil, and T. Setälä, Dimensionality of random light fields, J. Eur. Opt. Soc.-Rapid Publ. **13**, 36 (2017).
[24] M. A. Alonso, Geometric descriptions for the polarization of nonparaxial light: A tutorial, Adv. Opt. Photonics **15**, 176 (2023).
[25] K. Y. Bliokh and F. Nori, Transverse and longitudinal angular momenta of light, Phys. Rep. **592**, 1 (2015).
[26] J. J. Gil, A. Norrman, A. T. Friberg, and T. Setälä, Spin of random stationary light, Phys. Rev. A **107**, 053518 (2023).
[27] L. Bellando, M. Kleine, Y. Amarouchene, M. Perrin, and Y. Louyer, Giant diffusion of nanomechanical rotors in a tilted washboard potential, Phys. Rev. Lett. **129**, 023602 (2022).
[28] F. van der Laan, Rotational levitodynamics, Ph.D. thesis, ETH Zurich, 2022.
[29] M. Kamba, R. Shimizu, and K. Aikawa, Nanoscale feedback control of six degrees of freedom of a near-sphere, arXiv:2303.02831.
[30] See Supplemental Material at http://link.aps.org/supplemental/10.1103/PhysRevLett.132.253601 for theoretical considerations, which include Refs. [31–37].
[31] E. W. Weisstein, Euler angles, From MathWorld–A Wolfram Web Resource, https://mathworld.wolfram.com/EulerAngles.html.
[32] L. Novotny and B. Hecht, *Principles of Nano-Optics*, 2nd ed. (Cambridge University Press, Cambridge, England, 2012).
[33] I. Toftul, G. Fedorovich, D. Kislov, K. Frizyuk, K. Koshelev, Y. Kivshar, and M. Petrov, Nonlinearity-induced optical torque, Phys. Rev. Lett. **130**, 243802 (2023).
[34] R. Kitamura, L. Pilon, and M. Jonasz, Optical constants of silica glass from extreme ultraviolet to far infrared at near room temperature, Appl. Opt. **46**, 8118 (2007).
[35] F. Monteiro, S. Ghosh, E. C. van Assendelft, and D. C. Moore, Optical rotation of levitated spheres in high vacuum, Phys. Rev. A **97**, 051802(R) (2018).
[36] M. Schuck, D. Steinert, T. Nussbaumer, and J. W. Kolar, Ultrafast rotation of magnetically levitated macroscopic steel spheres, Sci. Adv. **4**, e1701519 (2018).
[37] D. Hümmer, R. Lampert, K. Kustura, P. Maurer, C. Gonzalez-Ballestero, and O. Romero-Isart, Acoustic and optical properties of a fast-spinning dielectric nanoparticle, Phys. Rev. B **101**, 205416 (2020).
[38] L. D. Landau and E. M. Lifshitz, *Mechanics, Third Edition: Volume 1 (Course of Theoretical Physics)*, 3rd ed. (Butterworth-Heinemann, London, 1976).
[39] A. D. Rider, C. P. Blakemore, A. Kawasaki, N. Priel, S. Roy, and G. Gratta, Electrically driven, optically levitated microscopic rotors, Phys. Rev. A **99**, 041802(R) (2019).
[40] H. Goldstein, C. Poole, and J. Safko, *Classical Mechanics*, 3rd ed. (Pearson Education, Boston, 2001).
[41] J. Gieseler, B. Deutsch, R. Quidant, and L. Novotny, Subkelvin parametric feedback cooling of a laser-trapped nanoparticle, Phys. Rev. Lett. **109**, 103603 (2012).
[42] J. A. Zielińska, F. van der Laan, A. Norrman, M. Rimlinger, R. Reimann, L. Novotny, and M. Frimmer, Controlling optomechanical libration with the degree of polarization, Phys. Rev. Lett. **130**, 203603 (2023).
[43] L. Martinetz, K. Hornberger, and B. A. Stickler, Gas-induced friction and diffusion of rigid rotors, Phys. Rev. E **97**, 052112 (2018).
[44] iXblue, blueSeis-3A Portable rotational 3-component seismometer, absolute and broadband (2022), https://www.ixblue.com/wp-content/uploads/2022/02/blueSeisdatasheet.pdf.
[45] C. Gonzalez-Ballestero, M. Aspelmeyer, L. Novotny, R. Quidant, and O. Romero-Isart, Levitodynamics: Levitation and control of microscopic objects in vacuum, Science **374**, eabg3027 (2021).
[46] Y. Ma, K. E. Khosla, B. A. Stickler, and M. S. Kim, Quantum persistent tennis racket dynamics of nanorotors, Phys. Rev. Lett. **125**, 053604 (2020).
[47] A. Frisk Kockum, A. Miranowicz, S. De Liberato, S. Savasta, and F. Nori, Ultrastrong coupling between light and matter, Nat. Rev. Phys. **1**, 19 (2019).
[48] J. Koch, G. R. Hunanyan, T. Ockenfels, E. Rico, E. Solano, and M. Weitz, Quantum Rabi dynamics of trapped atoms far in the deep strong coupling regime, Nat. Commun. **14**, 954 (2023).